Journal of the Korean Nuclear Society
Volume 28, Number 1, February 1996

Development of A Methodology for In-Reactor Fuel Rod Supporting Condition Prediction

K.T. Kim, H.K. Kim, and K.H. Yoon
Korea Atomic Energy Research Institute
(Received August 2, 1995)

노내 연료봉 지지조건 예측 방법론 개발

김규태 · 김형구 · 윤경호
한국원자력연구소
(1995. 8. 2 접수)

Abstract

The in-reactor fuel rod support conditions against the fretting wear-induced damage can be evaluated by residual spacer grid spring deflection or rod-to-grid gap. In order to evaluate the impact of fuel design parameters on the fretting wear-induced damage, a simulation methodology of the in-reactor fuel rod supporting conditions as a function of burnup has been developed and implemented in the GRIDFORCE program. The simulation methodology takes into account cladding creep rate, initial spring deflection, initial spring force, and spring force relaxation rate as the key fuel design parameters affecting the in-reactor fuel rod supporting conditions. Based on the parametric studies on these key parameters, it is found that the initial spring deflection, the spring force relaxation rate and cladding creepdown rate are in the order of the impact on the in-reactor fuel rod supporting conditions. Application of this simulation methodology to the fretting wear-induced failure experienced in a commercial plant indicates that this methodology can be utilized as an effective tool in evaluating the capability of newly developed cladding materials and/or new spacer grid designs against the fretting wear-induced damage.

요 약

프레팅마모 기인 연료봉 손상을 방지할 수 있는 노내 연료봉 지지조건은 잔여 지지격자 스프링 변위량 또는 연료봉/지지격자 갭에 의해 평가될 수 있다. 핵연료 설계인자들이 프레팅마모 손상에 미치는 영향을 평가하기 위해 연소도의 함수로서 노내 연료봉 지지조건을 모사할 수 있는 방법론을 사용하여 GRIDFORCE 프로그램을 개발하였다. 이 프로그램에서는 노내 연료봉 지지조건에 영향을 주는 주요 인자로서 피복관 크립, 초기 스프링 변위, 초기 스프링힘 그리고 스프링힘 조사이완이 고려된다. 이 주요 인자들에 대한 민감도 분석 결과, 초기 스프링 변위, 스프링힘 조사이완, 피복관 크립 순으로 노내 연료봉 지지조건에 영향을 주는 것으로 나타났다. 이 프로그램을 실제 노내에서 발생한 프레팅마모 기인 연료봉 손상에 적용한 결과를 토대로 판단해 볼 때 이 프로그램은 새로 개발된 피복관 재질 및/또는 새로 개발

된 지지격자 설계가 프레팅마모 기인 연료봉 손상을 방지할 수 있는 설계여유도를 효과적으로 평가할 수 있음을 알 수 있다.

1. Introduction

One of the aims of fuel designs is the assurance of the fuel rod and fuel assembly integrity under the normal operating conditions. Due to fuel design and/or its specifications deficiency, manufacturing fault, fuel handling or operational mistake, however, fuel failures have occurred. In the 1970s, the main failure mechanisms are identified as hydriding, PCI and clad collapsing, which were eliminated by corrective actions such as fuel design change and/or operational guideline improvement[1, 2, 3]. Recently, reasonably good fuel operating experience makes fuel vendors move to employ high burnup fuel with much confidence[4, 5, 6, 7]. It is noteworthy that waterside cladding corrosion and fuel rod internal overpressure due to accumulated fission gas release are the two limiting parameters for utilization of the fuel to high burnup[8]. This is why the corrosion-resistant cladding such as extra low tin Zry-4 [9] or new Zr base alloy[10] and pellets with less fission gas release such as ADS-doped pellet[11] have been developed. In addition, some fuel vendors have changed spacer grid design and/or material to optimize the performance of high burnup fuel[9, 12].

Recently one of the Westinghouse improved fuel assemblies of VANTAGE5H has suffered fretting wear induced fuel failure which may be caused by the lack of the fuel rod support by the spacer grid spring against the flow-induced vibration[13]. Regarding the fretting wear problems, key factors can be divided into two groups such as fuel design parameters and reactor hydraulic design parameters. The fuel design parameter includes initial spring deflection, irradiation-induced spring force relaxation, cladding creepdown and thermal expansion difference between spacer grid and rod. The reactor hydraulic design parameters are assemblywise flow distribution, axial flow rate fluctuation in the fuel assembly and cross flow rate at the interfaces of fuel assembly/fuel assembly and fuel assembly/baffle. It is well known that the probability of the fretting wear damage may be reduced by smaller cladding creepdown and spring force relaxation, larger initial spring deflection and lower flow-induced vibration. It is reported that the corrosion-resistant cladding may generate higher cladding creep rate than the standard Zry-4 cladding[14]. And improved spacer grid design with mixing vanes may cause unexpectedly large flow-induced vibration. These design changes needed for the high burnup fuel will deteriorate the capability against the fretting wear-induced failure. With the introduction of new cladding materials and new spacer grid designs, this makes it necessary to develop a model which can predict the fuel rod supporting conditions versus burnup.

In this work, a simulation methodology of the rod-to-grid supporting conditions will be developed and implemented in the GRIDFORCE program. With the help of this program, the impact of the fuel design parameters on the grid-to-rod supporting conditions will be evaluated, based on the parametric study. However, the impact of the reactor hydraulic design parameters on the fretting wear damage under the given grid-to-rod supporting conditions will not be evaluated since up to now there have existed no in-reactor vibration-related data of the fuel rod and the fuel assembly needed for benchmarking it.

2. Description of Methodology

It is well known that the fuel rod supporting conditions in a pressurized water reactor depend on the various parameters such as the cladding creep rate, the spacer grid design, and the coolant flow condition. In this work, however, only the effects of the cladding creep rate and the spacer grid design on the fretting wear-induced failure are considered. The

cladding creep rate depends on compressive stress of the fuel rod, the amount of fast fluence and the fuel rod temperature. The compressive stress is caused by the coolant system overpressure. The higher compressive stress, the larger fast fluence and the higher temperature will generate the larger fuel rod creepdown. The cladding creep rate can be predicted by a fuel performance code with the consideration of the fuel rod power histories and the thermal-hydraulic conditions. The initial spring deflection and force are determined by a spring force-deflection curve which is governed by the spring design such as spring height, spring width and spring shape. The spring force relaxation depends on the residual stress in spring and the amount of fast fluence. The higher residual stress and the larger fast fluence will generate the larger spring force relaxation. It is noteworthy that the cladding creepdown rate has a direct impact on the spring relaxation rate since the former controls the rod-to-grid gap size, i.e., the residual stress in spring. The simulation methodology developed in this work, which takes into account the cladding creep rate, the spring stiffness, the initial spring deflection, the initial spring force, and the spring force relaxation rate, can be described as follows:

The residual spring force at t=t at the operating temperature may be represented by the Hooke's law:

$$F_{RES}(t) = C_{OT}\ \delta_{RES}(t) \quad (1)$$

where $F_{RES}(t)$ = residual spring force at t=t

C_{OT} = spring constant at operating temperature

$\delta_{RES}(t)$ = residual elastic spring deflection at t=t

The spring constant at the operating temperature, C_{OT}, may be evaluated with the aid of the spring constant at the room temperature and spring elastic modulus when the spring constant at operating temperature is not available.

$$C_{OT} = (E_{OT} / E_{RT})\ C_{RT} \quad (2)$$

where C_{RT} = spring constant at room temperature

E_{OT} = spring elastic modulus at operating temperature

E_{RT} = spring elastic modulus at room temperature

As shown in Fig. 1, initial spring elastic deflection at the room temperature, δ_O, decreases due to the cladding elastic deflection caused by the coolant over pressure(δ_P) and the thermal expansion difference between the spacer grid strip and the cladding(δ_T). In addition, δ_O decreases with an increase of burnup due to the cladding creepdown(δ_{CR}), the spacer grid strip irradiation growth(δ_{IR}), the spring force relaxation(δ_{REX}). With the combination of all the parameters described above, the residual elastic spring deflection at t=t, $\delta_{RES}(t)$, may be given in the followings:

$$\delta_{RES}(t) = \delta_O - \delta_P(t) - \delta_T(t) - \delta_{CR}(t) - \delta_{IR}(t) - \delta_{REX}(t) \quad (3)$$

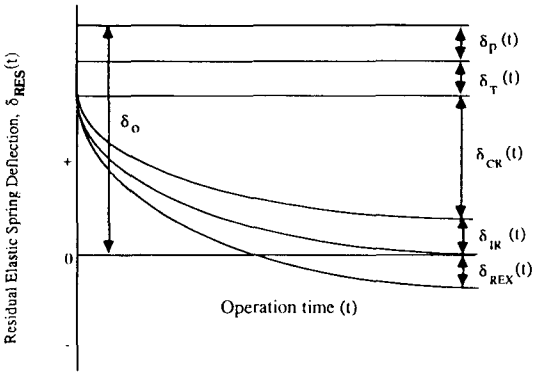

where $\delta_{RES}(t)$ = residual elastic spring deflection at t=t

δ_O = initial elastic spring deflection at room temp.

$\delta_P(t)$ = accumulated elastic cladding deflection caused by the coolant overpressure from t=0 to t=t

$\delta_T(t)$ = accumulated thermal expansion deflection between the spacer grid strip and the cladding from t=0 to t=t

$\delta_{CR}(t)$ = accumulated cladding creepdown from t=0 to t=t

$\delta_{IR}(t)$ = accumulated spacer grid irradiation growth from t=0 to t=t

$\delta_{REX}(t)$ = accumulated loss of elastic spring deflection due to spring force relaxation from t=0 to t=t

Fig. 1. Schematic Diagram of Residual Elastic Spring Deflection Versus Time.

The value of δ_O can be determined by an unstrained spring height, fuel rod pitch and initial cladding diameter. $\delta_P(t)$, $\delta_T(t)$, $\delta_{CR}(t)$ and $\delta_{IR}(t)$ can be calculated by the reactor operating conditions. Since the total spring deflection is decreased due to cladding creepdown and/or spacer grid irradiation growth, however, the value of $\delta_{REX}(t)$ for the spacer grid spring contacting on the cladding can not be determined directly by a burnup-dependent relaxation curve which is derived from in-pile spring force relaxation tests performed under a constant total (elastic+plastic) spring deflection. In order to evaluate the impact of a burnup-dependent total spring deflection on the amount of the spring force relaxation, a time-weighted spring force may be introduced for the calculation of the residual spring force :

$$F_{RES}(t) = F_G(t) - [1 - R(t)]\, F^{W}_{EFF}(t) \quad (4)$$

where $F_{RES}(t)$ = residual spring force at t=t

$F_G(t)$ = spring force calculated by the geometrical configuration of cladding and spacer grid at t=t without considering spring force relaxation

$R(t)$ = fraction of residual spring force to be relaxed from t=0 to t=t, which is derived under a constant total (elastic+plastic) spring deflection condition

$F^{W}_{EFF}(t)$ = time-weighted spring force from t=0 to t=t

Using the relationship of $F=C\,\delta$, equation (4) can be rewritten as

$$\delta_{RES}(t) = \delta_G(t) - [1 - R(t)]\, \delta^{W}_{RES}(t) \quad (5)$$

where $\delta_G(t)$ = elastic spring deflection calculated by the geometrical configuration of cladding and spacer grid at t=t without considering spring force relaxation

$= \delta_O - \delta_P(t) - \delta_T(t) - \delta_{CR}(t) - \delta_{IR}(t)$

$\delta^{W}_{RES}(t)$ = time-weighted elastic spring deflection calculated by the geometrical configuration of cladding and spacer grid from t=0 to t=t without considering spring force relaxation

Comparison of equation (3) and (5) shows

$$\delta_{REX}(t) = [1 - R(t)]\, \delta^{W}_{RES}(t) \quad (6)$$

With the introduction of time-weighted values of δ^{W}_P, δ^{W}_T, δ^{W}_{CR} and δ^{W}_{IR}, $\delta^{W}_{RES}(t)$ can be given as :

$$\delta^{W}_{RES}(t) = \delta_O - \delta^{W}_P(t) - \delta^{W}_T(t) - \delta^{W}_{CR}(t) - \delta^{W}_{IR}(t) \quad (7)$$

$\delta^{W}_P(t)$ = time-weighted elastic cladding deflection caused by the coolant overpressure from t=0 to t=t

$\delta^{W}_T(t)$ = time-weighted thermal expansion difference between the spacer grid and the cladding from t=0 to t=t

$\delta^{W}_{CR}(t)$ = time-weighted cladding creepdown from t=0 to t=t

$\delta^{W}_{IR}(t)$ = time-weighted spacer grid irradiation growth from t=0 to t=t

$\delta^{W}_P(t)$, $\delta^{W}_T(t)$, $\delta^{W}_{CR}(t)$ and $\delta^{W}_{IR}(t)$ may be defined as follows :

$$\delta^{W}_P(t) = \frac{1}{t}\int_0^t \delta^{*}_P(\tau)\left[\frac{t-\tau}{t}\right] d\tau \quad (8)$$

$$\delta^{W}_T(t) = \frac{1}{t}\int_0^t \delta^{*}_T(\tau)\left[\frac{t-\tau}{t}\right] d\tau \quad (9)$$

$$\delta^{W}_{CR}(t) = \frac{1}{t}\int_0^t \delta^{*}_{CR}(\tau)\left[\frac{t-\tau}{t}\right] d\tau \quad (10)$$

$$\delta^{W}_{IR}(t) = \frac{1}{t}\int_0^t \delta^{*}_{IR}(\tau)\left[\frac{t-\tau}{t}\right] d\tau \quad (11)$$

where $\delta^*_P(\tau)$ = increment of the elastic cladding deflection caused by the coolant overpressure at $t=\tau$

$\delta^*_T(\tau)$ = increment of the thermal expansion difference between cladding and spacer grid at $t=\tau$

$\delta^*_{CR}(\tau)$ = increment of the cladding creep-down at $t=\tau$

$\delta^*_{IR}(\tau)$ = increment of the spacer grid irradiation growth at $t=\tau$

It is noted that in the above equations the weighting factor of $[t-\tau]$ is introduced to consider the impact of $\delta^*_P(\tau)$, $\delta^*_T(\tau)$, $\delta^*_{CR}(\tau)$ and $\delta^*_{IR}(\tau)$ on the amount of the spring force relaxation. This weighting factor represents an elapsed time from $t=\tau$ $t=t$ after the appearance of $\delta^*_P(\tau)$, $\delta^*_T(\tau)$, $\delta^*_{CR}(\tau)$ and $\delta^*_{IR}(\tau)$ at $t=\tau$. In order to simplify the integration in the above equations, the time of t is divided into N time intervals and then the integral given in the above equations can be transformed into a summation :

$$\delta^W_P(t) = \sum_{j=1}^{N} [\delta_P(j) - \delta_P(j-1)] [t_N - (t_j - 1/2\Delta t_j)]/t_N \quad (12)$$

$$\delta^W_T(t) = \sum_{j=1}^{N} [\delta_T(j) - \delta_T(j-1)] [t_N - (t_j - 1/2\Delta t_j)]/t_N \quad (13)$$

$$\delta^W_{CR}(t) = \sum_{j=1}^{N} [\delta_{CR}(j) - \delta_{CR}(j-1)] [t_N - (t_j - 1/2\Delta t_j)]/t_N \quad (14)$$

$$\delta^W_{IR}(t) = \sum_{j=1}^{N} [\delta_{IR}(j) - \delta_{IR}(j-1)] [t_N - (t_j - 1/2\Delta t_j)]/t_N \quad (15)$$

where Δt_j = time interval at the (j)th time step $= t_j - t_{j-1}$

Then, substitution of equation (7) and equations (12) through (15) into equation (5) gives

$$\delta_{RES}(t) = \delta_G(t) - [1-R(t)][\delta_o - \delta^W_P(t) - \delta^W_T(t) - \delta^W_{CR}(t) - \delta^W_{IR}(t)] \quad (16)$$

The above equations (1) through (16) have been implemented into the GRIDFORCE computer program. With the aid of this program, the fuel rod supporting conditions as a function of burnup can be easily predicted when the fuel assembly design parameters are known.

3. Application

According to the fretting wear-induced damage observed in a Korean nuclear power plant, some fuel rods have experienced the rod-to-grid fretting wear-induced failure during the second residence time. The first symptom of the fuel failure due to the rod-to-grid fretting wear occurred at 20-23 MWD /kgU, which corresponds to about 100 days after the startup of the second residence time. Due to the different flow-induced vibration in the core and in the fuel assembly, however, some fuel rods even in the failed fuel assemblies and some fuel assemblies located at the symmetric positions of the failed fuel assemblies have remained intact. This indicates that the flow conditions in the core and in the assembly has a considerable impact on the fretting wear-induced damage. With the assumption of the worst flow conditions in the core and in the assembly, however, the GRIDFORCE program developed in this work was employed to simulate the fretting wear-induced damage observed in the Korean nuclear power plant. According to the visual examination of the rod-to-grid fretting wear profile versus spacer grid at 35 MWD/kgU, as shown in Fig. 2, the rod-to-grid fretting wear appears to be the largest at the 4th and the 5th grid positions and propagates in the lower grid positions rather than in the upper grid positions. With the aid of the GRIDFORCE program, the residual elastic spring deflections as a function of bur-

nup were calculated at various grid positions, as shown in Fig. 3. From this figure, it can be seen that the rod-to-grid gap initiates at the 5th and the 6th grid positions at the burnup of about 22 MWD/kgU. Then, the rod-to-grid gap propagates in the direction of the lower grid positions with an increase of burnup. This may explain that the largest fretting wear occurs at the 4th and the 5th grid positions even if the largest rod-to-grid gap forms at the 5th and the 6th grid positions. The 1st grid position shows larger fretting wear than the 2nd grid position since the fuel rod region at below the 1st grid position is free-ended and experiences usually high cross flow due to the entrance effect at the bottom end piece region. On the other hand, the reason of the rod-to-grid gap propagation in the direction of the lower grid positions is that the 7th and the 8th grids locate at the interface of the fuel/non-fuel region and in the non-fuel(plenum) region, respectively, where relatively very low are fast neutron fluence and cladding creep-down which are key factors for generating the rod-to-grid gap.

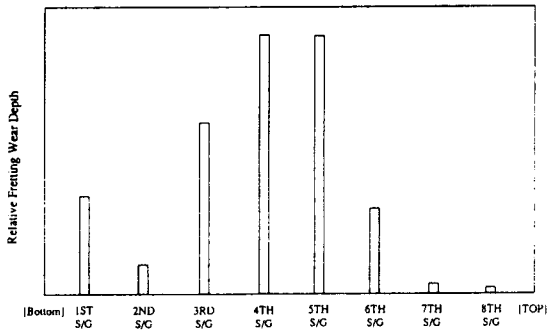

Fig. 2. Fretting Wear Depth Profile Versus Spacer Grid Observed in a Nuclear Power Plant with the Grid-to-Rod Fretting-Induced Failure.

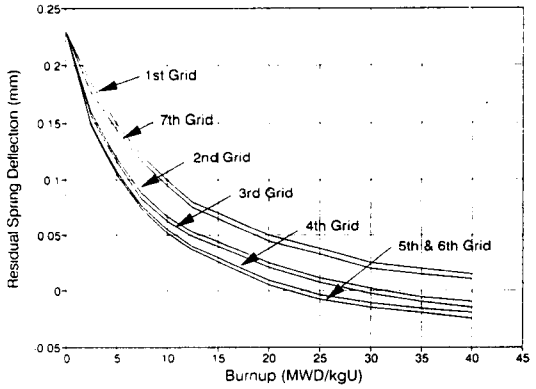

Fig. 3. Burnup-Dependent Residual Spring Deflection at Various Grid Positions for a Fuel Type with the Fretting Wear-Induced Damage, Predicted by the GRIDFORCE Program.

Considering that measured data of the rod-to-grid gap at the onset of the fretting wear damage are not available, an explicit guideline of the minimum rod-to-grid gap against the fretting wear damage can not be determined. For the Inconel spacer grid considered in this work, therefore, it is assumed that the onset of the rod-to-grid gap formation will initiate the fretting wear. With the use of this assumption, comparison of the rod-to-grid gap profile at about 35 MWD/kgU shown in Fig. 3 and the fretting wear dep th profile shown in Fig. 2 indicates that the GRIDFORCE program is considered to be a good tool in evaluating the capability of a spacer grid design against the fretting wear damage.

4. Parametric Study

With the aid of the GRIDFORCE program containing the simulation model developed in this work, the parametric studies on the key parameters of the fuel rod supporting conditions such as the cladding creep-down, the initial spring deflection, the initial spring force, and the spring force relaxation have been performed. The spring characteristic curves of the typical spring designs employed in this work are given in Fig. 4. From this figure, it can be seen that depending on spring type the spring deflection varies from 0.3 to 1.0 mm and the initial spring force from 7 to

27 N. The typical spring force relaxation rates are given in Fig. 5. Depending on the spring design, the remaining fractional spring force at 8×10^{21} n/cm^2 varies from 0.3 to 0.1. The typical creepdown behaviors of the cladding tubes supplied to the Korean nuclear plants are given in Fig. 6. These curves indicate that the lower tin content generates the faster creepdown. Based on the given data in Figs. 4 through 6, the GRIDFORCE program can evaluate the effect of each parameters on the fuel rod supporting conditions. In this work, the fuel rod supporting conditions at the middle spacer grid position have been investigated since the fretting wear-induced fuel damage started at the middle spacer grid position, as shown in Fig. 2.

4.1. Initial Spring Deflection

Fig. 4 shows the spring deflection-force curves employed in this work [15]. In order to evaluate the effect of only the initial spring deflection on the fuel rod supporting conditions, the spring type B was selected. From Fig. 4, it can be seen that the tolerance range of spring deflection is from 0.3 to 1.0 mm. As

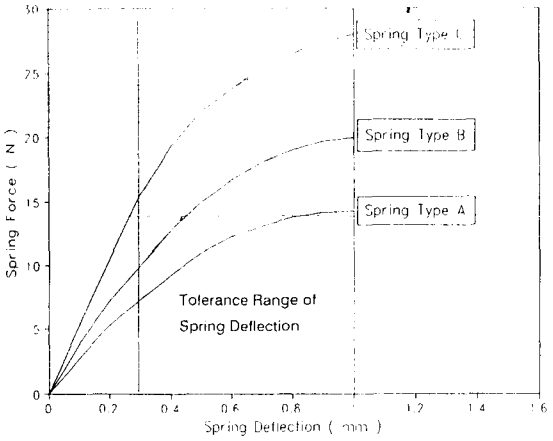

Fig. 4. Spring Characteristic Curves for Three Spring Types Used in This Work

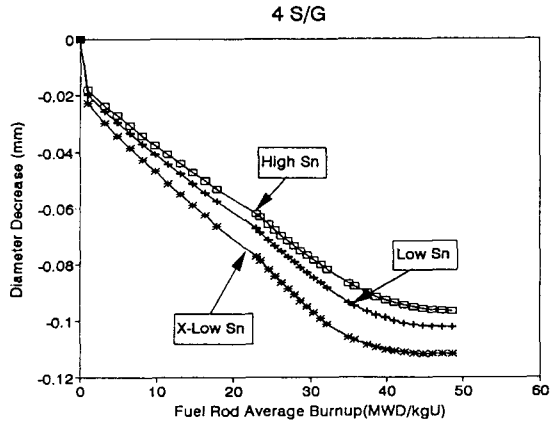

Fig. 6. Cladding Creepdown Rates for Three Cladding Tubes Used in This Work.

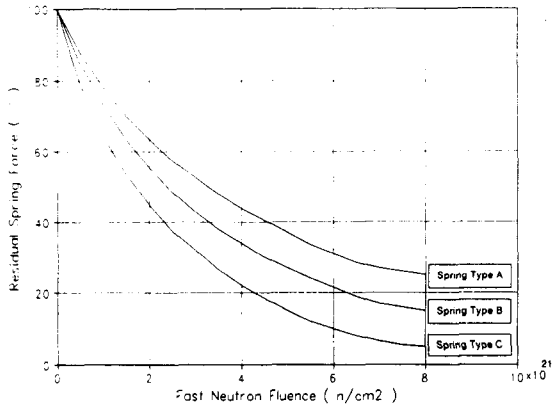

Fig. 5. Spring Force Relaxation Rates for Three Spring Types Used In This Work, Derived Under a Constant Total Spring Deflection Condition.

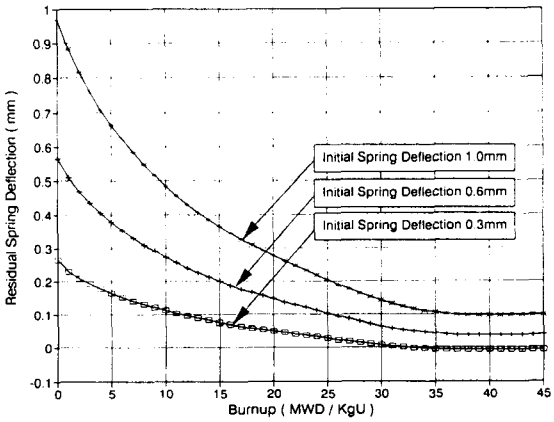

Fig. 7. Effect of Initial Spring Deflection on Residual Spring Deflection.

an input datum in the GRIDFORCE program, three initial spring deflections of 0.3, 0.6, 1.0 mm were selected from the tolerance range of the spring type B. The results for the effect of the initial spring deflection is shown in Fig. 7. From this figure, it can be seen that the larger spring deflection generates the larger residual spring deflection, as expected. The initial spring deflection of 0.3 mm generates gap from fuel rod burnup of 32 MWD/kgU, whereas the initial spring deflection of 1.0 mm does not generates gap and residual spring deflection is saturated to be 0.1 mm from 38 MWD/kgU. Therefore, it is recommended that the lower tolerance range of spring deflection for new spring designs be checked whether or not the rod-to-grid gap will form during the fuel lifetime, which can be easily checked by the GRIDFORCE program.

4.2. Initial Spring Force

In order to evaluate the effect of only the initial spring force on the fuel rod supporting conditions, the same relaxation curve and cladding creepdown were employed regardless of spring design. As an input datum in the GRIDFORCE program, three initial spring forces of 7, 10, 15 N with the same spring deflection of 0.3 mm were selected from Fig. 4. The results for the effect of the initial spring force is show n in Fig. 8. From this figure, it can be seen that there is nearly no effect of the initial spring force on the residual spring deflection behavior. According to the results predicted by the GRIDFORCE program, it can be said that, in order to improve the spacer grid design against the fretting wear-induced failure, one should increase the initial spring deflection rather than the initial spring force.

4.3. Spring Force Relaxation

Three kinds of spring force relaxation rate used in this work [15] are given in Fig. 5. In order to evaluate the effect of only the spring force relaxation on the fuel rod supporting conditions, the same initial spring deflection and cladding creepdown were employed regardless of the spring force relaxation. As an input datum in the GRIDFORCE program, three spring force relaxation rates were selected from Fig. 5. The results for the effect of the spring force relaxation is shown in Fig. 9. From this figure, it can be seen that the smaller spring force relaxation generates the larger residual spring deflection, as expected. The spring relaxation types B and C generate gap from the fuel rod burnup of 33 and 26

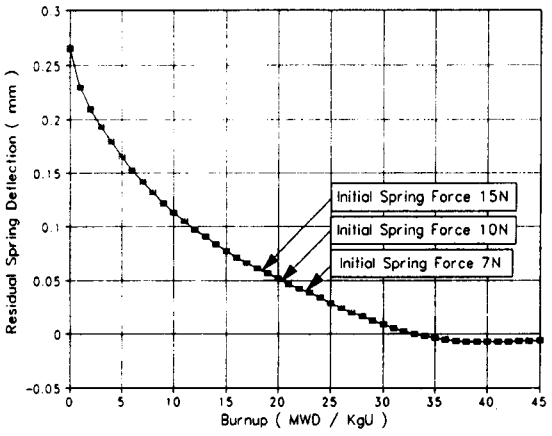

Fig. 8. Effect of Initial Spring Force on Residual Spring Deflection.

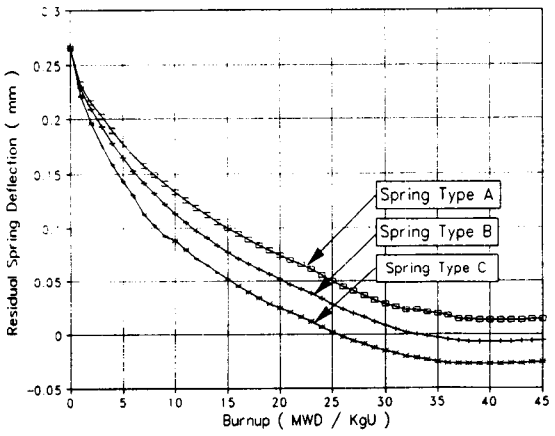

Fig. 9. Effect of Spring Force Relaxation Rate on Residual Spring Deflection.

MWD/kgU, respectively, whereas the spring relaxation type A does not generate gap and residual spring deflection is saturated to be 0.02 mm from 38 MWD/kgU. According to the results predicted by the GRIDFORCE program, it can be said that, in order to improve the spacer grid design against the fretting wear-induced failure, one should reduce the spring force relaxation as small as possible. Considering that the higher local stress in the spring generates the faster spring force relaxation, it is recommended that local stress in the spring be reduced by optimizing spring shape.

4.4. Cladding Creepdown

Three cladding creepdown curves used in this work [16] are given in Fig. 6. In order to evaluate the effect of only the cladding creepdown on the fuel rod supporting conditions, the same initial spring deflection and spring force relaxation were employed. As an input datum in the GRIDFORCE program, three cladding creepdowns were selected from Fig. 6. The results for the effect of the cladding creepdown is shown in Fig. 10. From this figure, it can be seen that the smaller cladding creepdown generates the larger residual spring deflection, as expected. The extra low tin cladding generates gap from the fuel rod burnup of 30 MWD/kgU, whereas the high tin cladding generates gap from the fuel rod burnup of 35 MWD/kgU.

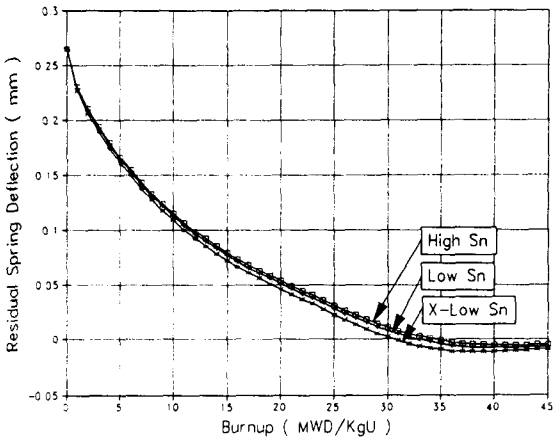

Fig. 10. Effect of Cladding Creepdown Rate on Residual Spring Deflection.

Comparison of the effect of each parameter on the residual spring deflection indicates that the most important parameter is the initial spring deflection and the second one is the spring force relaxation. It also indicates that the initial spring force does not affect the residual spring deflection behavior if the same initial spring deflection is used. In order to optimize the spacer grid design against the fretting wear-induced failure, therefore, one should have a spacer grid design of relatively low spring force but large spring deflection since it is generally known that the larger initial spring force shows the faster spring force relaxation due to higher local stress in the spring. In addition, one should use the cladding material with small creepdown rate if the other performance parameters such as oxidation and irradiation growth are not concerned.

5. Conclusions

A simulation methodology for the evaluation of the impact of the fuel design on the fuel rod support conditions has been developed and implemented in the GRIDFORCE program. The GRIDFORCE program has been considered to simulate well the fretting wear profile versus spacer grid positions as a function of burnup. Based on the parametric studies, it is found that the most dominant parameter for the residual spring deflection is the initial spring deflection and the second one is the spring force relaxation. It is also found that the initial spring force does not affect the residual spring deflection behavior. In order to optimize the existing spacer grid designs and/or develop new spacer grid designs, the GRIDFORCE program can be employed as an effective tool since it will check whether or not a proposed spacer grid design can prevent the fretting wear-induced damage.

References

1. D.H. Locke, Review of Experience with Water Reactor Fuels 1968-1973, Nuclear Engineering and Design, 33 (1975) 94
2. P. Knudsen, Evaluation of LWR Fuel Performance under Transient and Off-Normal Conditions : A Review of Recent Reports, RISO-M-221 1 (1979)
3. M. Gaetner and G. Fischer, Survey of the Power Ramp Performance Testing of KWU's PWR UO_2 Fuel, J. of Nuclear Materials 149 (1987)
4. M.G. Andrews et al, Operating Experience with Combustion Engineering Fuel at High Burnups, ANS Topical Meeting on LWR Extended Burnup-Fuel Performance and Utilization Virginia, April (1982)
5. H.W. Wilson et al, Fuel Performance Characteristics at Extended Burnup, ANS Topical Meeting on LWR Extended Burnup-Fuel Performance and Utilization (Virginia, April (1982)
6. D.E. Bentley et al, High Burnup Performance of Exxon Nuclear Company Fuel in the H.B. Robinson Pressurized Water Reactor, ANS Topical Meeting on LWR Extended Burnup-Fuel Performance and Utilization (Virginia, April (1982)
7. H. Stehlem et al, KWU Experience and Analysis of LWR Fuel with respect to High Burnup, ANS Topical Meeting on LWR Extended Burnup-Fuel Performance and Utilization (Virginia, April (1982)
8. C.E. Beyer and R. Lobel, Licensing Fuel for Extended Burnup Operation, ANS Transactions, 54 (1987)
9. R. Holzer et al, Fuel Design Advancements by Application of Siemens FOCUS Technology, The 7th KAIF/KNS Annual Conference (1992)
10. R.S. Miller et al, Westinghouse Fuel Operating at High Burnup and with Advanced Features, International Topical Meeting on LWR Fuel Performance (1994)
11. Y.W. Lee, et al., The Development of ADS-doped UO2 Pellet Technology for High Burnup Nuclear Fuel, KAERI/TR-381/93 (1993)
12. D.L. Stucker, Nuclear Fuel Design Considerations for the 1990s, The 8th KAIF/KNS Annual Conference (1993)
13. Washington, Fuel Failure at Two Plants Force Westinghouse to Redesign VANTAGE5H, Nuclear Fuel, 18 (1993)
14. W.A. McInteer, et al., The Influence of Tin Content on the Thermal Creep of Zircaloy-4, ASTM STP 1023 (1989)
15. Borsdorf, Verification of Fuel Rod Support in Fuel Assemblies with Inconel Spacer Grids Type AH 42, KWU BT52/93/E346
16. Manual for a Computer Code CARO-D, Fuel Performance Analysis Code, KAERI, 1989